



Published in final edited form as:

J Comput Neurosci. 2009 October ; 27(2): 201. doi:10.1007/s10827-009-0137-7.

Analysis of Nerve Conduction Block Induced by Direct Current

Changfeng Tai¹, James R. Roppolo², and William C. de Groat²

¹ Department of Urology, University of Pittsburgh, Pittsburgh, PA 15261, USA

² Department of Pharmacology and Chemical Biology, University of Pittsburgh, Pittsburgh, PA 15261, USA

Abstract

The mechanisms of nerve conduction block induced by direct current (DC) were investigated using a lumped circuit model of the myelinated axon based on Frankenhaeuser-Huxley (FH) model. Four types of nerve conduction block were observed including anodal DC block, cathodal DC block, virtual anodal DC block, and virtual cathodal DC block. The concept of activating function was used to explain the blocking locations and relation between these different types of nerve block. Anodal/cathodal DC blocks occurred at the axonal nodes under the block electrode, while virtual anodal/cathodal DC blocks occurred at the nodes several millimeters away from the block electrode. Anodal or virtual anodal DC block was caused by hyperpolarization of the axon membrane resulting in the failure of activating sodium channels by the arriving action potential. Cathodal or virtual cathodal DC block was caused by depolarization of the axon membrane resulting in inactivation of the sodium channel. The threshold of cathodal DC block was lower than anodal DC block in most conditions. The threshold of virtual anodal/cathodal blocks was about 3–5 times higher than the threshold of anodal/cathodal blocks. The blocking threshold was decreased with an increase of axonal diameter, a decrease of electrode distance to axon, or an increase of temperature. This simulation study, which revealed four possible mechanisms of nerve conduction block in myelinated axons induced by DC current, can guide future animal experiments as well as optimize the design of electrodes to block nerve conduction in neuroprosthetic applications.

Keywords

Axon; direct current; nerve block; model

I. INTRODUCTION

It is well known that anodal DC current applied to nerves can block the conduction of action potentials [1][2]. Anodal block has been used in neurophysiological studies to block large diameter axons in nerves allowing only small axons to conduct action potentials [3]–[5]. Because most studies employing DC block often used bipolar electrodes (i.e. one electrode was anode and the other was cathode), it is uncertain whether the axonal block occurs at the anodal electrode or the cathodal electrode [1]–[8]. Some studies [6][7] provided evidence showing that DC block occurs under the cathodal electrode rather than the anodal electrode. This view was supported by a recent study [9] employing both computer simulation and electrophysiological methods, which indicated that the DC block was primarily due to depolarization of the nerve membrane under the cathodal electrode.

DC block can be easily observed in animal experiments using isolated nerves by determining whether the action potentials can propagate through the region where the block electrode is located [1]–[8]. However, it is very difficult to determine the blocking mechanism and the precise blocking location along the nerve in animal experiments since it will require recording neural activity at each axonal node near the blocking electrode, including not only membrane potentials but also ionic currents. Computer simulation employing an axonal model has the advantage of analyzing activity at every node along an axon, but such detailed analysis is currently still not available in animal experiments. In this study we analyzed the DC block induced by a monopolar point electrode using a myelinated axonal model. Membrane potentials, ionic currents, and ionic channel activity were analyzed node-by-node at the region close to the blocking electrode. Understanding the mechanism and location of DC block induced by a monopolar point electrode could provide the basic concepts and knowledge that could be used to guide a more complex design of stimulating electrode in neuroprosthetic applications [10]–[12].

II. METHODS

Axonal Model

The nerve model used in this study is shown in Fig. 1. A 60 mm long, myelinated axon is modeled with the inter-node length $\Delta x = 100d$ (where d is the axon diameter). Each node (nodal length: $L = 2.5 \mu\text{m}$) is modeled by a membrane capacitance (C_m) and a variable membrane resistance (R_m). The ionic currents passing through the variable membrane resistance are described by FH model [13][14]. Two monopolar point electrodes (with the indifferent electrode at infinity) are placed at 1 mm distance from the axon (Fig. 1). One is the block electrode at the 40 mm location along the axon, where the DC blocking current will be delivered. The other is the test electrode at the 10 mm location, which will deliver a uniphasic single pulse (pulse width 0.1 ms and intensity varying from 0.5 mA to 2 mA) to evoke an action potential and test whether this action potential can propagate through the site of the block electrode. The test electrode will always be a cathode (negative pulse), and the block electrode will deliver either anodic DC or cathodic DC depending on the purpose of the study. The test pulse is always delivered at 2 ms after the start of the DC blocking current.

We assume that the axon is in an infinite homogeneous medium (resistivity $\rho_e = 300 \Omega\text{cm}$). After neglecting the small influence induced by the presence of the axon in the homogeneous medium, the extracellular potential $V_{e,j}$ at the j^{th} node along the axon can be calculated by:

$$V_{e,j}(t) = \frac{\rho_e}{4\pi} \left[\frac{I_{block}(t)}{\sqrt{(j\Delta x - x_0)^2 + z_0^2}} + \frac{I_{test}(t)}{\sqrt{(j\Delta x - x_1)^2 + z_1^2}} \right]$$

where $I_{block}(t)$ is the DC current delivered to the block electrode (at location $x_0 = 40 \text{ mm}$, $z_0 = 1 \text{ mm}$); $I_{test}(t)$ is the single test pulse delivered to the test electrode (at location $x_1 = 10 \text{ mm}$, $z_1 = 1 \text{ mm}$).

The change of the membrane potential V_j at the j^{th} node is described by:

$$\frac{dV_j}{dt} = \left[\frac{d\Delta x}{4\rho_i L} \left(\frac{V_{j-1} - 2V_j + V_{j+1}}{\Delta x^2} + \frac{V_{e,j-1} - 2V_{e,j} + V_{e,j+1}}{\Delta x^2} \right) - I_{i,j} \right] / c_m$$

where $V_j = V_{i,j} - V_{e,j} - V_{rest}$; $V_{i,j}$ is the intracellular potential at the j^{th} node; $V_{e,j}$ is the extracellular potential at the j^{th} node; V_{rest} is the resting membrane potential; ρ_i is the resistivity of axoplasm

(100 Ωcm); c_m is the capacity of the membrane (2 $\mu\text{F}/\text{cm}^2$); $I_{i,j}$ is the ionic current at the j^{th} node described by FH equations [13][14].

The axonal model was solved by Runge-Kutta method [15] with a time step of 0.001 ms. The simulation always started at initial condition $V_j = 0$. The membrane potentials (both transmembrane potential V_j and extracellular potential $V_{e,j}$) at the two end nodes of the modeled axon were always equal to the membrane potentials of their closest neighbors, which implemented the sealed boundary conditions (no longitudinal currents) at the two ends of the modeled axon. The simulations were performed with the temperature parameter set at 37 $^{\circ}\text{C}$ if not specified.

Activating Function

The activating function f_j at the j^{th} node introduced by Rattay [16][17] is defined as:

$$f_j = \frac{V_{e,j-1} - 2V_{e,j} + V_{e,j+1}}{\Delta x^2}$$

which explains the influence of an externally applied electrical field on a targeted axon. The activating functions generated by a single point electrode (either cathodic or anodic) along an axon in an infinite homogeneous medium are schematically plotted in Fig. 2. The axonal region with a positive f_j will be depolarized, whereas a negative f_j will hyperpolarize the axonal membrane. A cathodal electrode can induce membrane depolarization under the electrode and at the nodes very close to the electrode, while inducing hyperpolarization at the nodes further away from the electrode (i.e. at the “side lobe” region, see Fig. 2). Similarly, an anodal electrode can hyperpolarize the axonal membrane in the center area, while depolarizing the membrane at the “side lobe” region. Although only a single point electrode is used in this model, the depolarization or hyperpolarization in the “side lobe” region could be assumed to be induced by a virtual anode for the cathodal point electrode, and by a virtual cathode for the anodal point electrode (Fig. 2). The concept of activating function will be used in this study to explain the DC block phenomenon.

III. RESULTS

The axonal model as shown in Fig. 1 successfully simulated the nerve conduction block induced by a DC current. Four different types of DC blocks were observed including anodal DC block (Fig. 3), cathodal DC block (Fig. 4), virtual anodal DC block (Fig. 5), and virtual cathodal DC block (Fig. 6) depending on the polarity of the electrode and the intensity of the DC current. The blocking mechanisms and locations are analyzed in detail in the following sections.

Anodal DC Block

Fig. 3A shows that the action potential initiated by the test electrode (at 10 mm location after applying the DC blocking current for 2 ms) was propagating toward the block electrode. The propagation of this action potential was blocked by an anodal DC current (0.8 mA) delivered to the block electrode (at 40 mm location) from the beginning. Fig. 3B–G show the change of membrane potential, ionic current, and ion channel activity at every axonal node near the block electrode during the anodal DC block shown in Fig. 3A. Membrane hyperpolarization was maximal at the node under the block electrode and declined in a gradual manner at nodes of increasing distance from the block electrode (see Fig. 3B). The membrane hyperpolarization under the block electrode was so strong that the arriving action potential could not depolarize the membrane enough to activate the sodium channels (Fig. 3E, $m=0$) resulting in no inward sodium current (Fig. 3C) and the conduction failure (Fig. 3A). Meanwhile, the potassium

channels were closed (Fig. 3G, $n=0$) and there was no potassium current (Fig. 3D) at the node under the electrode. Therefore, the anodal DC block occurred at the node under the block electrode due to the failure of sodium channel activation.

Cathodal DC Block

Fig. 4A shows that the action potential initiated by the test electrode was blocked by a cathodal DC current (0.4 mA). In contrast to the anodal DC current (Fig. 3A), the cathodal DC current induced an initial action potential at the beginning of its application that was propagating in both directions (Fig. 4A). After the initial action potential the cathodal DC current constantly depolarized the membrane and blocked the propagation of the action potential induced by the test electrode. Fig. 4B–G show the change of membrane potential, ionic current, and ion channel activity at every axonal node near the block electrode during the cathodal DC block as shown in Fig. 4A. The axonal membrane was maximally depolarized under the block electrode (see Fig. 4B) and exhibited a gradually decreasing depolarization at axonal nodes at greater distances from the block electrode. The membrane depolarization under the block electrode caused a complete inactivation of the sodium channel (Fig. 4F, $h=0$) resulting in no sodium current when the action potential arrived at the node under this electrode (Fig. 4C). The potassium channel was constantly open (Fig. 4G) resulting in large outward potassium current (Fig. 4D) when the action potential arrived at the block electrode. Therefore, the cathodal DC block occurred at the node under the block electrode due to inactivation of the sodium channels.

Virtual Anodal DC Block

Fig. 5A shows a nerve conduction block induced by cathodal DC current (1.1 mA) at a location about 2–3 mm away from the block electrode (i.e., at locations of 37–38 mm along the axon) where the membrane was maximally hyperpolarized (Fig. 5B). This hyperpolarization was due to the virtual anodal effect of the cathodal electrode (Fig. 2). It is worth noting that the virtual anode induced hyperpolarization also prevented the initial action potential induced by the cathodal DC current from propagating away from the cathodal electrode (Fig. 5A), whereas this initial action potential could propagate when the cathodal DC current was low (0.4 mA, Fig. 4A). The virtual anodal effect was so strong that the arriving action potential could not depolarize the membrane enough to activate the sodium channels (Fig. 5E, $m=0$) resulting in no inward sodium current (Fig. 5C) and the conduction failure (Fig. 5A). Meanwhile, the potassium channels were closed (Fig. 5G, $n=0$) and there was no potassium current at the virtual anode (Fig. 5D). Therefore, when the cathodal DC current was of sufficient intensity, the virtual anodal DC block could occur at the nodes about 2–3 mm away from the block electrode due to the failure of sodium channel activation.

Virtual Cathodal DC Block

Similar to the virtual anodal block, virtual cathodal block could also occur when the anodal DC current is at high intensity. Fig. 6A shows a virtual cathodal block induced by an anodal DC current (2.5 mA) at a location about 3–4 mm away from the block electrode (i.e., at locations of 36–37 mm along the axon) where the membrane was maximally depolarized (Fig. 6B). This depolarization was due to the virtual cathodal effect of the anodal electrode (Fig. 2). It is worth noting that the virtual cathode induced depolarization also produced an initial action potential propagating away from the block electrode (Fig. 6A), whereas no initial action potential was produced when the anodal DC current was low (0.8 mA, Fig. 3A). The virtual cathodal effect caused a complete inactivation of the sodium channel (Fig. 6F, $h=0$) and no sodium current when the action potential arrived at the nodes depolarized by the virtual cathode (Fig. 6C). The virtual cathodal depolarization also induced a constant opening of the potassium channel (Fig. 6G) and a large potassium current (Fig. 6D). Therefore, virtual cathodal DC block can occur

at the nodes about 3–4 mm away from the block electrode by inactivation of sodium channels when the anodal DC current was of sufficient intensity.

Threshold of DC Block

The threshold for anodal or cathodal block was influenced by axon diameter (Fig. 7A), electrode distance to the axon (Fig. 7B), and the temperature (Fig. 7C). Large axons have a lower blocking threshold than small axons (Fig. 7A). Increasing the electrode distance to the axon requires more current to block conduction (Fig. 7B). At a low temperature range (15–25 °C) the blocking threshold is constant, but declines at a high temperature (37 °C) (Fig. 7C). It is worth noting that the threshold for cathodal block is lower than the threshold for anodal block except for a large diameter axon (20 μm , Fig. 7A), at a close electrode distance (1 mm, Fig. 7B), or at a high temperature (37 °C, Fig. 7C).

IV. DISCUSSION

In this study, we investigated the possible mechanisms underlying axonal conduction block induced by DC current in myelinated axons using the FH model. Four types of conduction block were identified including anodal DC block (Fig. 3), cathodal DC block (Fig. 4), virtual anodal DC block (Fig. 5), and virtual cathodal DC block (Fig. 6). The anodal/cathodal DC block occurred at the axonal nodes under the block electrode (Fig. 3–4), but the virtual anodal/cathodal DC block occurred at the nodes about 2–4 mm away from the block electrode (Fig. 5–6). The threshold of cathodal DC block was always lower than the threshold of anodal DC block in most conditions (Fig. 7). The blocking threshold was higher for smaller axons and for a larger electrode distance to the axon (Fig. 7A–B). The influence of temperature on blocking threshold was only observed at a higher temperature of 37 °C (Fig. 7C), which decreased the threshold. Understanding the DC block of nerve conduction could provide a very useful guide to design stimulation electrodes for neuroprosthetic applications [10]–[12].

The thresholds of virtual anodal/cathodal DC block were not determined in this study. They were about 3–5 times higher than the threshold of anodal/cathodal DC block. As the intensity of DC current increased, there was always a transition from a cathodal (or anodal) block under the block electrode to a virtual anodal (or cathodal) block adjacent to the block electrode (Fig. 2). It was very difficult to determine the exact threshold when the virtual anodal (or cathodal) block occurred since the transition occurred gradually. The threshold of anodal/cathodal DC block could be easily determined by the failure of the action potential to propagate through the site of the block electrode. But this criterion could not be applied to determine the threshold of virtual anodal/cathodal DC block because the anodal/cathodal DC block had already occurred under the block electrode. Therefore, Figs. 5 and 6 only showed the virtual anodal and cathodal blocks when the DC current was at an intensity that produced an unambiguous block. This also indicates that it would be very difficult in physiological experiments [1]–[9] to determine if a nerve conduction block was a cathodal (or anodal) DC block or a virtual anodal (or cathodal) DC block, since at a low current intensity it could be the former but at a high current intensity it could shift to a virtual block. Therefore, the DC block observed in animal experiments was probably due to either depolarization or hyperpolarization under the block electrode or on the side of the electrode (see Fig. 2) depending on the intensity and polarity of the DC current.

Only a monopolar electrode was analyzed in this study in order to simplify the complex nerve block phenomena observed in animal experiments and analyze the basic mechanisms and blocking locations. However, bipolar and tripolar electrodes were often used in animal experiments to block the nerve conduction [1]–[9]. The activating function produced by a bipolar/tripolar stimulating electrode will be more complex than that produced by a monopolar electrode. However, the basic principles for DC block as revealed in this study should still be

applicable, i.e. the anodal/cathodal DC block will occur under an individual electrode while virtual anodal/cathodal DC block should occur adjacent to electrode depending on electrode polarity and current intensity. It is worth noting that the activating function produced by a bipolar/tripolar electrode in the animal experiments [1]–[9] would also be influenced by the distances between the individual electrodes and by the inhomogeneity of the medium surrounding the nerve and electrodes [16][17]. These factors could significantly change the shape of the activating function in different animal experiments even if the same electrode designs were used (i.e. bipolar or tripolar), creating additional uncertainty about the mechanism of DC block that was reported in previous animal experiments [1]–[9]. Thus, quantitative study to record from the axonal nodes around the stimulation electrode using either microelectrode or optical imaging technologies is warranted, so that the nodal activity similar to what was shown in this study (Figs. 3–6) could be investigated during DC block in animal experiments.

Nerve conduction block induced by extracellularly applied DC current has been studied by other investigators [9] using both FH [14] and MRG models [18]. It was reported that the anodal DC block did not occur because the virtual cathodal DC block had a lower blocking threshold and always occurred before the anodal DC block [9]. However, it was not reported whether the result was from MRG model or from FH model. The result in our study demonstrated clearly using FH model that anodal DC block can occur before virtual cathodal DC block (Fig. 3 and Fig. 6). In previous study [9] in order to determine the location of the conduction block only the amplitude of the action potential was used. However, the amplitude of action potential gradually decreases along the axon during DC block causing difficulties in identifying the location and type of the conduction block (see Figs. 3–6). Therefore, in this study membrane potentials as well as the ionic currents and ionic gating parameters were used to identify the blocking mechanisms and determine the blocking locations. Similar studies using other myelinated or unmyelinated axonal models [18]–[22] are needed to confirm the results presented in this study and to reveal other possible mechanisms of DC block.

This simulation analysis has revealed that nerve conduction block induced by DC current should not be determined simply as anodal or cathodal DC block based on the polarity of the electrode as most often described in previous animal studies [1]–[8]. It also demonstrated the usefulness of computer simulation in situations where it is difficult to obtain reliable data in animal experiments. The results obtained in this simulation study should be useful in the design of animal experiments to obtain further support for our conclusions. This simulation study will also be very helpful in designing stimulation electrodes to be used in neuroprosthetic devices for people with disabilities [10]–[12].

Acknowledgments

This work is supported by the NIH under grants R56-DK-068566, R01-NS-051671, and R01-DK-077783.

References

1. Kuffler SW, Gerard RW. The small-nerve motor system to skeletal muscle. *J Neurophysiol* 1947;10:383–394.
2. Petruska JC, Hubscher CH, Johnson RD. Anodally focused polarization of peripheral nerve allows discrimination of myelinated and unmyelinated fiber input to brainstem nuclei. *Exp Brain Res* 1998;121:379–390. [PubMed: 9746144]
3. Whitwam JG, Kidd C. The use of direct current to cause selective block of large fibers in peripheral nerves. *Br J Anaesth* 1975;47:1123–1133. [PubMed: 1218139]
4. Mendell LM, Wall PD. Presynaptic hyperpolarization: a role for fine afferent fibers. *J Physiol* 1964;172:274–294. [PubMed: 14205021]

5. Hopp FA, Zuperku EJ, Coon RL, Kampine JP. Effect of anodal blockade of myelinated fibers on vagal C-fiber afferents. *Amer J Physiol* 1980;239:R454–462. [PubMed: 7435661]
6. Sassen M, Zimmermann M. Differential blocking of myelinated nerve fibers by transient depolarization. *Pflugers Arch* 1973;341:179–195. [PubMed: 4737412]
7. Zimmermann M. Selective activation of C-fibers. *Pflugers Arch, Gesamte Physiol Menschen Tiere* 1968;301:329–333.
8. Manfredi M. Differential block of conduction of larger fibers in peripheral nerve by direct current. *Arch Ital Biol* 1970;108:52–71. [PubMed: 5438721]
9. Bhadra N, Kilgore KL. Direct current electrical conduction block of peripheral nerve. *IEEE Trans Neural Syst Rehabil Eng* 2004;12:313–324. [PubMed: 15473193]
10. Loeb GE. Neural prosthetic interfaces with the nervous system. *Trends in Neurosci* May;1989 12(5): 195–201.
11. Roth BJ. Mechanisms of electrical stimulation of excitable tissue. *Critical Rev Biomed Eng* 1994;22:253–305. [PubMed: 8598130]
12. Tai C, Jiang D. Selective stimulation of smaller fibers in a compound nerve trunk with single cathode by rectangular current pulses. *IEEE Trans Biomed Eng* 1994;41:286–291. [PubMed: 8045582]
13. Rattay F, Aberham M. Modeling axon membranes for functional electrical stimulation. *IEEE Trans Biomed Eng* 1993;40:1201–1209. [PubMed: 8125496]
14. Frankenhaeuser B, Huxley AF. The action potential in the myelinated nerve fibre of *Xenopus Laevis* as computed on the basis of voltage clamp data. *J Physiol (Lond)* 1964;171:302–315. [PubMed: 14191481]
15. Boyce, WE.; Dprima, RC. *Elementary Differential Equations and Boundary Value Problems*. 6. John Wiley & Sons, Inc; 1997. p. 436-457.
16. Rattay F. Current distance relations for fiber stimulation with pointsources. *IEEE Trans Biomed Eng* 2008;55:1122–1127. [PubMed: 18334404]
17. Rattay F. Analysis of models for extracellular fiber stimulation. *IEEE Trans Biomed Eng* 1989;36:676–682. [PubMed: 2744791]
18. McIntyre CC, Richardson AG, Grill WM. Modeling the excitability of mammalian nerve fibers: Influence of afterpotentials on the recovery cycle. *J Neurophysiol* 2002;87:995–1006. [PubMed: 11826063]
19. Hodgkin AL, Huxley AF. A quantitative description of membrane current and its application to conduction and excitation in nerve. *J Physiol (Lond)* 1952;117:500–544. [PubMed: 12991237]
20. Chiu SY, Ritchie JM, Rogart RB, Stagg D. A quantitative description of membrane currents in rabbit myelinated nerve. *J Physiol (Lond)* 1979;292:149–166. [PubMed: 314974]
21. Schwarz JR, Eikhof G. Na currents and action potentials in rat myelinated nerve fibres at 20 and 37°C. *Pflugers Arch* 1987;409:569–577. [PubMed: 2442714]
22. Schwarz J, Reid G, Bostock H. Action potentials and membrane currents in the human node of ranvier. *Pflugers Arch Eur J Physiol* 1995;430(2):283–292. [PubMed: 7675638]

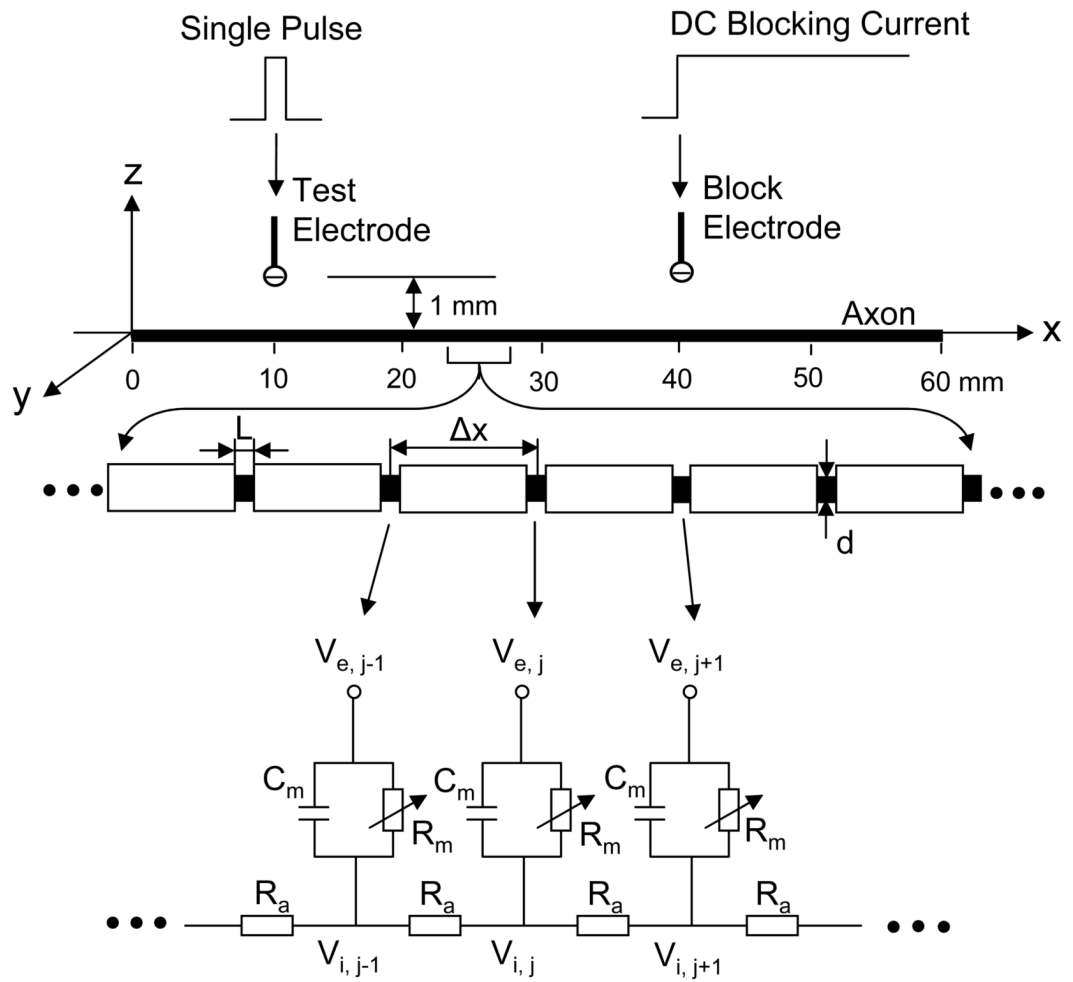


Fig. 1. Myelinated axonal model used to simulate conduction block induced by direct current (DC). The inter-node length $\Delta x = 100d$; d is the axon diameter. L is the nodal length. Each node is modeled by a resistance-capacitance circuit based on the FH model. R_a : inter-nodal axoplasmic resistance; R_m : nodal membrane resistance; C_m : nodal membrane capacitance; $V_{i,j}$: intracellular potential at the j th node; $V_{e,j}$: extracellular potential at the j th node.

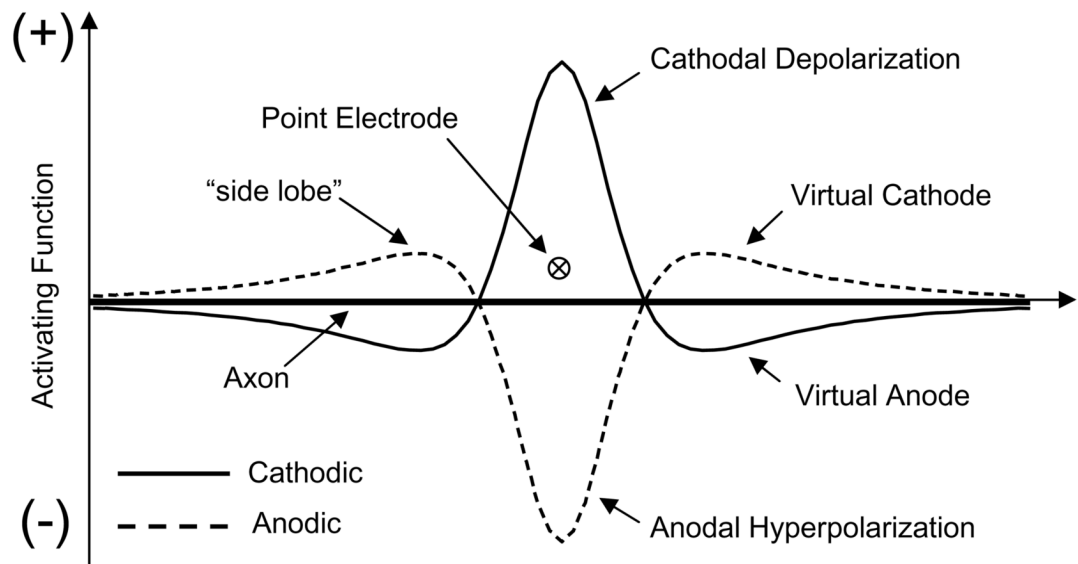


Fig. 2. Activating function generated by a point electrode along the axon. The axonal region where the activating function is positive will be depolarized, whereas the region where the activating function is negative will be hyperpolarized.

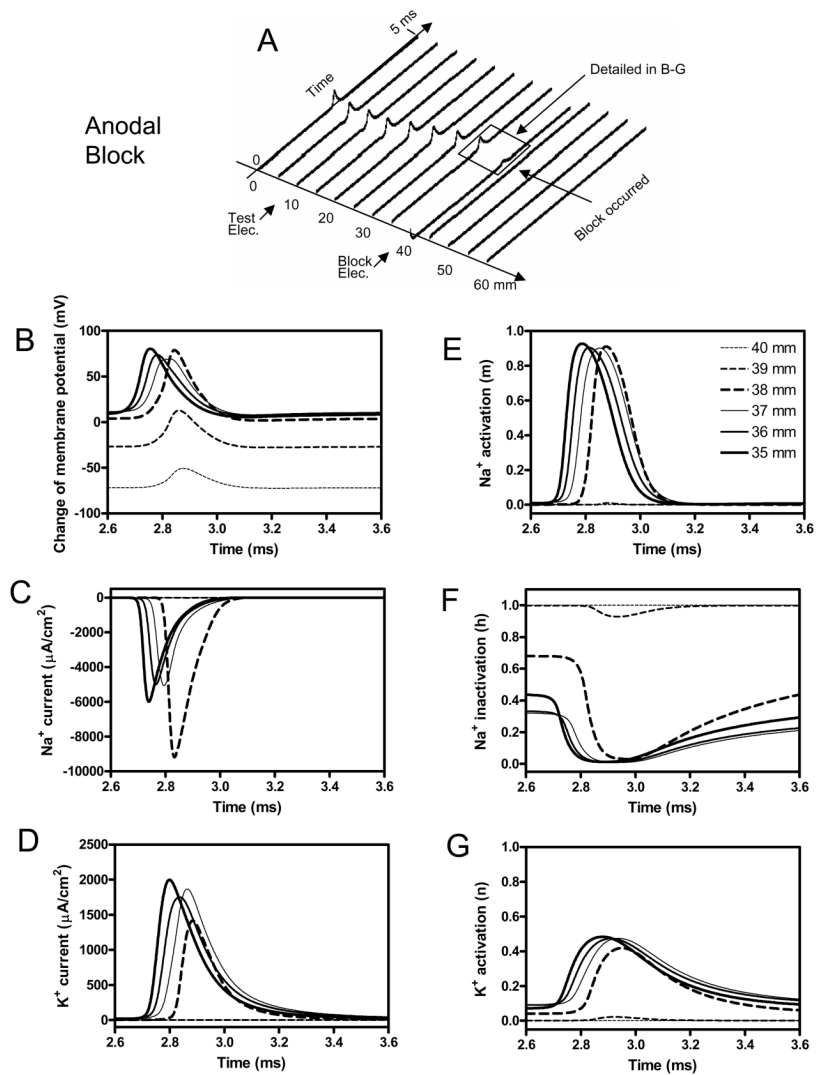


Fig. 3. Change of membrane potentials, ionic currents and activation/inactivation of the ion channels at different locations along the axon near the block electrode during anodal block. The legends in E indicate the locations along the axon. The intensity of the anodal DC current delivered to the block electrode at 40 mm location is 0.8 mA. Axon diameter: 10 μm. Distance from block electrode to axon: 1 mm.

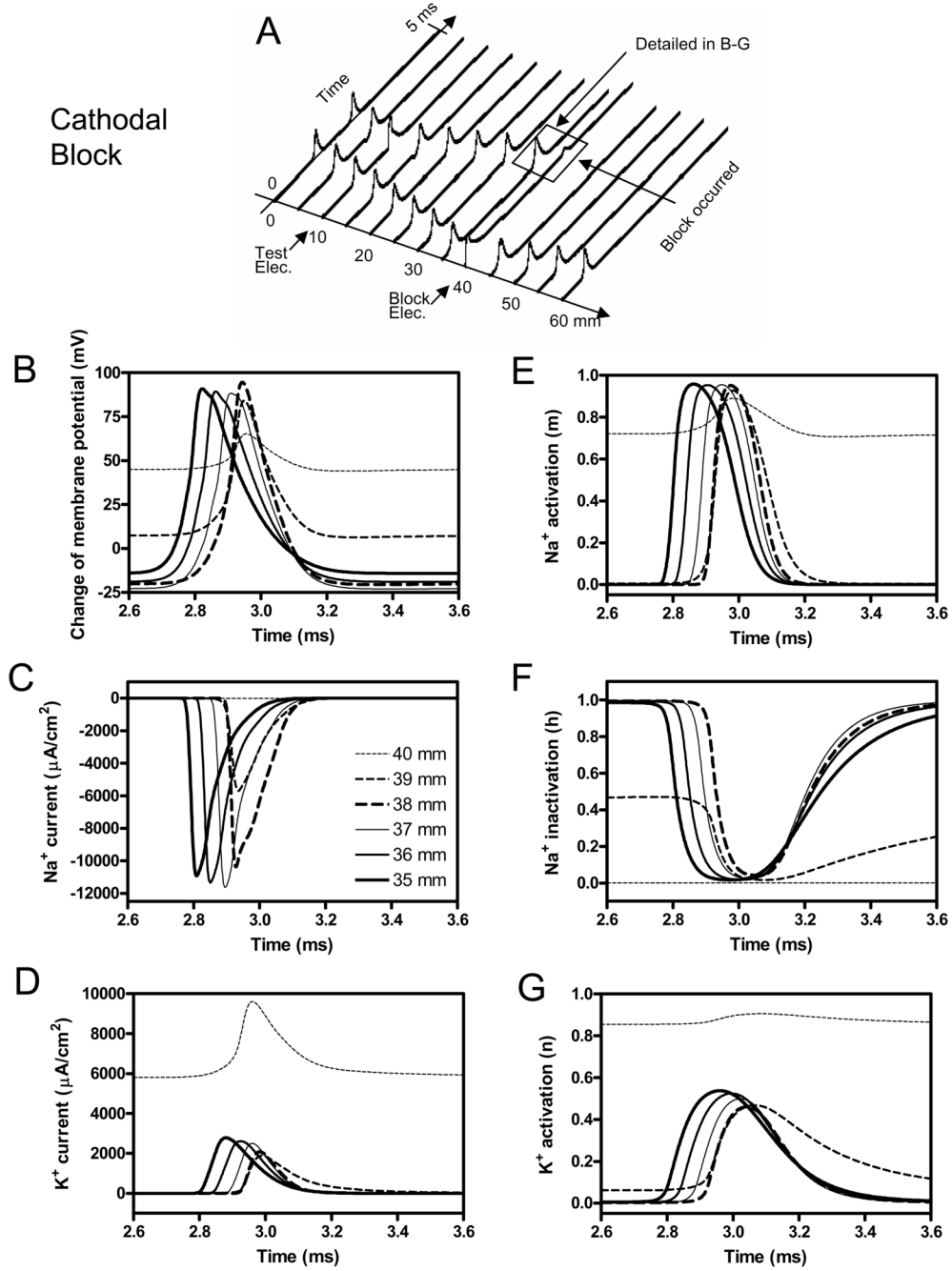


Fig. 4. Change of membrane potentials, ionic currents and activation/inactivation of the ion channels near the block electrode during cathodal block. The legends in C indicate the locations along the axon. The intensity of the cathodal DC current delivered to the block electrode at 40 mm location is 0.4 mA. Axon diameter: 10 μm. Distance from block electrode to axon: 1 mm.

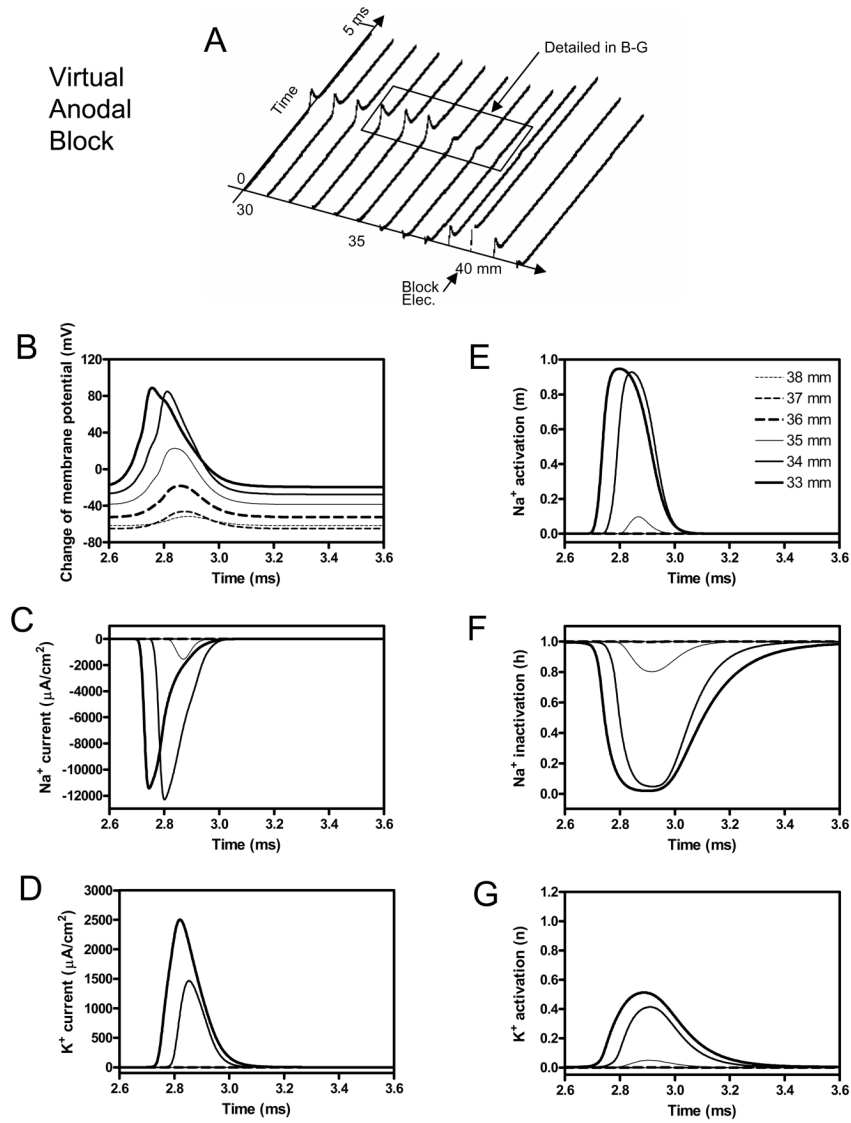


Fig. 5. Change of membrane potentials, ionic currents and activation/inactivation of the ion channels near the block electrode during virtual anodal block. The legends in E indicate the locations along the axon. The intensity of the cathodal DC current delivered to the block electrode at 40 mm location is 1.1 mA. Axon diameter: 10 μm. Distance from block electrode to axon: 1 mm.

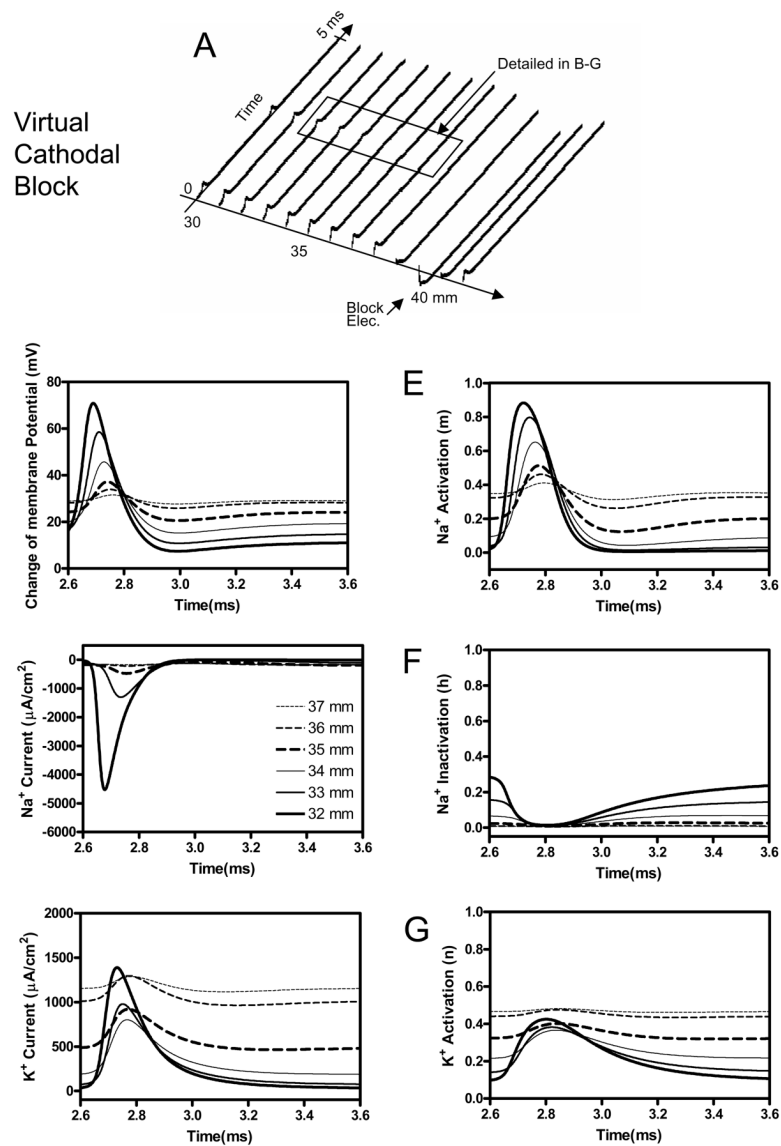


Fig. 6. Change of membrane potentials, ionic currents and activation/inactivation of the ion channels near the block electrode during virtual cathodal block. The legends in C indicate the locations along the axon. The intensity of the anodal DC current delivered to the block electrode at 40 mm location is 2.5 mA. Axon diameter: 10 μm. Distance from block electrode to axon: 1 mm.

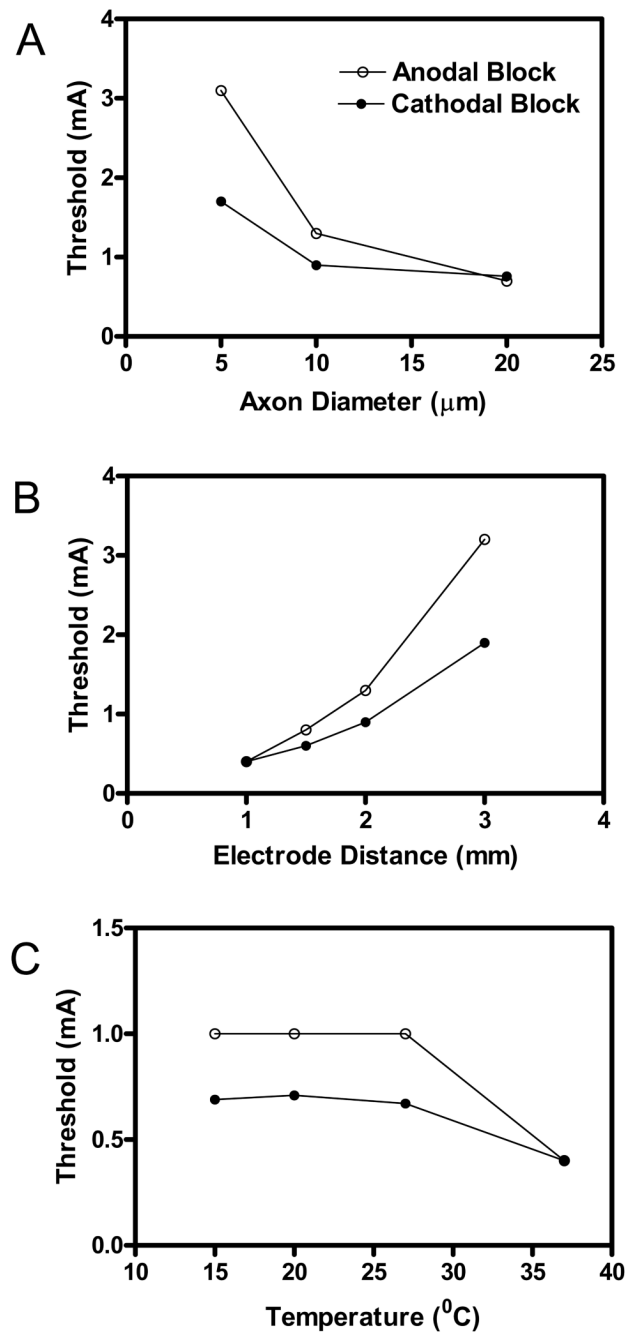


Fig. 7. The thresholds of anodal or cathodal block change with axon diameter (A), electrode distance (B), and temperature (C). A: electrode distance = 2 mm, temperature = 37 $^{\circ}\text{C}$. B: Axon diameter = 10 μm ; temperature = 37 $^{\circ}\text{C}$. C: electrode distance = 1 mm, axon diameter = 10 μm .